

# A Synthetic Electrocardiogram (ECG) Image Generation Toolbox to Facilitate Deep Learning-Based Scanned ECG Digitization

Kshama Kodthalu Shivashankara, Afagh Mehri Shervedani and Reza Sameni\*

**Abstract**—The electrocardiogram (ECG) is an accurate and widely available tool for diagnosing cardiovascular diseases. ECGs have been recorded in printed formats for decades and their digitization holds great potential for training machine learning (ML) models in algorithmic ECG diagnosis. Physical ECG archives are at risk of deterioration and scanning printed ECGs alone is insufficient, as ML models require ECG time-series data. Therefore, the digitization and conversion of paper ECG archives into time-series data is of utmost importance. Deep learning models for image processing show promise in this regard. However, the scarcity of ECG archives with reference time-series is a challenge. Data augmentation techniques utilizing *digital twins* present a potential solution. We introduce a novel method for generating synthetic ECG images on standard paper-like ECG backgrounds with realistic artifacts. Distortions including handwritten text artifacts, wrinkles, creases and perspective transforms are applied to the generated images, without personally identifiable information. As a use case, we generated an ECG image dataset of 21,801 records from the 12-lead PhysioNet PTB-XL ECG time-series dataset. A deep ECG image digitization model was built and trained on the synthetic dataset, and was employed to convert the synthetic images to time-series data for evaluation. The signal-to-noise ratio (SNR) was calculated to assess the image digitization quality vs the ground truth ECG time-series. The results show an average signal recovery SNR of  $27 \pm 2.8$  dB, demonstrating the significance of the proposed synthetic ECG image dataset for training deep learning models. The codebase is available as an open-access toolbox for ECG research.

**Index Terms**—Electrocardiogram (ECG), ECG digitization, deep learning, synthetic data, digital twins, data augmentation

## I. INTRODUCTION

Cardiovascular diseases (CVDs) are the primary cause of mortality globally among adults aged 37 to 70 years [1]. An electrocardiogram (ECG) is a representation of the cardiac electrical activity over time [2], and the most accessible and widely used tool for CVD diagnosis. The ECG is most accurately studied through standard multilead recordings (e.g., 12-lead). Every day, clinicians conduct millions of ECGs, and wearable and personal devices generate millions more. There are billions of digital diagnostic ECGs globally and billions more in conventional formats such as microfilms, printed papers and scanned images. Although this legacy

contains invaluable information on prevalent and rare CVDs and their evolution across generations and geography, we are not currently “learning” from ECG archives. Due to natural deterioration, lack of funding and a transition to digital ECGs, non-digital ECG archives worldwide will soon be destroyed, before we can learn from them. This will be an irreversible loss for CVD research, since the ECG is the only biological signal that has been recorded for over a century without significant changes in its acquisition protocol, especially for low and low middle income countries (LMICs), where paper ECGs are still more common. Although non-digital ECGs can be scanned and archived as images, there is little incentive to do so; because currently ECG images are not automatically searchable for anomalies, and are incompatible with annotation software that analyze ECG time-series [3]. Digitization of the existing paper ECG archives is an essential step in this context. ECG biomarkers, such as RR, PR, QRS, QT intervals, waveforms and rhythms are easily accessible from ECG time-series and could help better performance of existing machine learning models.

Further, paper ECGs are restricted mainly due to privacy concerns as they contain personal and sensitive information. The US HIPAA rule requires appropriate safeguards to protect the privacy of protected health information and sets limits and conditions on the uses and disclosures that may be made of such information without an individual’s consent [4]. This requires informed consent from each patient from whom the record has been procured, making the availability of open-source datasets scarce. Most datasets have been randomised or pseudonymised for de-identification of personally identifiable information [5]. However, there are significant concerns that de-identified datasets can be re-identified through linkage of metadata [6], or more recently through deep learning models [7]. Thus there have been many attempts to model ECG synthetically in a privacy-preserving manner to adhere to all privacy regulations while generating massive amounts of data. In this work, we focus on generating synthetic paper-like ECG images from ground truth time-series data to cater to applications such as ECG image digitization that may require large paper ECG datasets [8]. Synthetic data must contain all characteristics of the real data population without any personally identifiable information. Thus, we aim to mimic all possible distortions present in paper ECG records while generating images from time-series data. We present a step-by-step mechanism for generating distortionless paper ECG records from digital data, followed by sequentially adding distortions such as printed

K. Kodthalu Shivashankara is with the School of Electrical and Computer Engineering, Georgia Institute of Technology, Atlanta, GA, USA. A. Mehri Shervedani is with the Electrical and Computer Engineering Department, University of Illinois Chicago, Chicago, IL. R. Sameni is with the Department of Biomedical Informatics, Emory University, Atlanta, GA, USA. Corresponding author: R. Sameni ([rsameni@dbmi.emory.edu](mailto:rsameni@dbmi.emory.edu))

text artifacts, handwritten text, wrinkles, creases, perspective distortions, and environmental noise.

Our developed tool for synthetic ECG image generation (ECGGen) has been implemented in Python and is available online<sup>1</sup>.

## II. RELATED WORK

There is an increasing interest in the generation of realistic synthetic data and so-called *digital twins*. Privacy preservation and HIPAA mandates have forced researchers to look at synthetic medical data generation, particularly Electronic Health records (EHR). In [9], John et al. proposed using a federated generative adversarial network (GAN) to generate EHRs. The GAN was trained on real-world EHRs to generate a dataset of “fake” patients through synthetic data. Through medGAN [10], Choi et al. demonstrated the usability of a GAN in the generation of EHRs. EHR-Safe [11] is another synthetic EHR-data generation framework that aimed to model EHR data through a sequential encoder-decoder architecture and GANs.

In the ECG context, there are numerous research elucidating the generation of synthetic time-series ECG records. Previously, dynamical models have been used to produce synthetic ECG data of adults and fetuses [12], [13]. The model generates a trajectory for the ECG in a three-dimensional state space. The model parameters can be selected to generate different morphologies for the PQRST complex and heart rate. This model also captures morphological variabilities in the human ECG. In [14], Clifford et al. used an artificial vector model for generating abnormal ECG rhythms. The normal ECG is generated using a three-dimensional vectorcardiogram formulation, while abnormal beats are generated as perturbations to the expected trajectory. In [15] a general framework was presented for morphological modeling of ECG data using signal decomposition techniques. [16] demonstrated simulating sinus rhythm, episodes of atrial fibrillation, and atrial premature beats in ECGs. These simulations again use physical models to generate synthetic abnormalities.

There have been recent advancements in synthetic data generation using GANs. Zhu et al. [17] proposed using a GAN composed of a bidirectional long short-term memory(LSTM) and convolutional neural network(CNN) to generate synthetic ECG time-series. The generated synthetic time-series data exhibit properties that match existing clinical data and retain features of patients with CVDs. Delaney et al. [18] proposed a regular GAN-based architecture but utilized recurrent neural networks (RNN) and convolutional neural networks (CNN) to generate time-series ECG data. The generated time-series samples are structurally similar to their training sets and exhibit variabilities across samples. GANs have also been successfully shown to generate synthetic ECG with abnormalities. Zhang et al. [19] proposed a two-dimensional bidirectional LSTM GAN to produce 12-lead ECGs corresponding to four different conditions: left ventricular hypertrophy (LVH), left branch bundle block (LBBB), acute myocardial infarction (ACUTMI), and normal. In [20], Wulan introduced three generative

models for the generation of ECG signals — namely the WaveNet-based model, the SpectroGAN-based model, and the WaveletGAN model — to generate ECG signals with three different kinds of beats: normal, left bundle branch block and right bundle branch block. These research demonstrate that generating synthetic time-series ECG can be made possible through generative models. To leverage these advances for the development and validation of ECG image digitization algorithms, considerably large datasets of scanned paper ECG images and their corresponding ground truth time-series data are required. However, to date, large paper ECG archives are not readily available. In [21], Thambawita et al. used WaveGAN and Pulse2Pulse GAN to generate *DeepFake* ECGs and have created a repository with the resulting ECG images. The generated ECGs inherently have synthetic time-series data underlying the images and are validated using General Electric’s MUSE 12SL ECG interpretation program. Herein, we take a different approach to synthetic paper ECG generation. We focus on a privacy-preserving approach to synthetic ECG image generation by plotting ECG time-series data on standard paper ECG grids and adding artifacts and distortions sequentially. Therefore, synthetic paper-like ECG images are obtained for which the underlying ground-truth real ECG time-series are available. Thus, the dataset can be used to develop effective ECG image digitization algorithms of high accuracy.

## III. METHODOLOGY

The proposed methodology includes step-by-step addition of distortions to distortion-less time-series data plotted on standard ECG grids, as shown in Fig. 1. Each step of the developed pipeline is detailed in the sequel.

### A. The ECG time-series

The synthetic paper ECG generation pipeline requires a time-series dataset which functions as the ground truth. For this purpose, we use the PTB-XL dataset [22], a clinical ECG dataset which has been compiled for training machine learning algorithms with clear benchmark procedures. The dataset contains 21,801 clinical 12-lead ECGs from 18,869 patients of 10 second length. This dataset also contains extensive metadata and statistics on signal properties and demographics such as age, sex, height and weight. Each record is provided with the standard set of ECG leads I, II, III, aVR, aVL, aVF, V1, V2, V3, V4, V5 and V6 [22]. In addition to the PTB-XL dataset, we also use other 12-lead clinical ECG datasets such as the CPSC and the CPSC-Extra Databases [23], the INCART Database [24], the Georgia 12-lead ECG database (G12EC) and the PTB database [25]. These datasets were used as part of the 2021 PhysioNet Challenges on multilead ECG annotation [26]. The segments of interest are extracted as short 10s time-series arrays from the entire time-series data, lead-wise. All the leads are used to construct the standard 12 lead ECG. Most time-series records from the above mentioned datasets could be contaminated by various types of measurement noises such as baseline artifacts, power line interference, motion artifacts, muscle noise and additive white Gaussian noise (AWGN) [27]. These different forms of real ECG noises can be modeled and

<sup>1</sup>A link to the toolbox will be provided upon the acceptance of the manuscript.

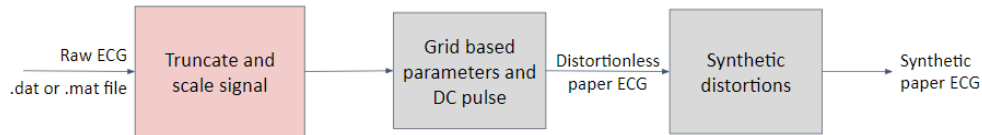


Fig. 1: Proposed pipeline for generating synthetic ECG images

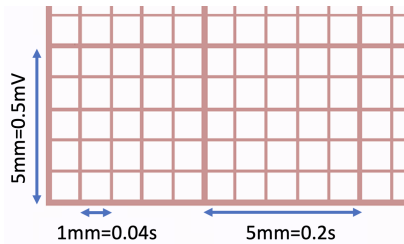


Fig. 2: The standard grid on printed ECG papers/images

added to time series data in order to make it more realistic [13]. Since realistic ECG noise is not white or stationary, most practical applications involving noise addition to time-series ECG data involves addition of real ECG noises such as those found in the MIT-BIH non-stress test database with varying signal-to-noise ratios [28]. Further, time-varying models such as autoregressive models can be used to simulate realistic ECG noise and can be added to time-series data, as mentioned in [13].

### B. The standard ECG paper

The standard printed ECG is recorded at 25 mm/sec speed and the standard vertical scale is such that 10 mm on the paper corresponds to 1 mV of physical units of the ECG. There are two grids plotted on the standard paper ECG: a coarse grid of 5 mm×5 mm corresponding to 0.5 mV in vertical (amplitude) and 0.2 s in horizontal (time) directions, and a fine grid of 1 mm×1 mm corresponding to 0.1 mV and 40 ms in vertical and horizontal directions, as shown in Fig. 2.

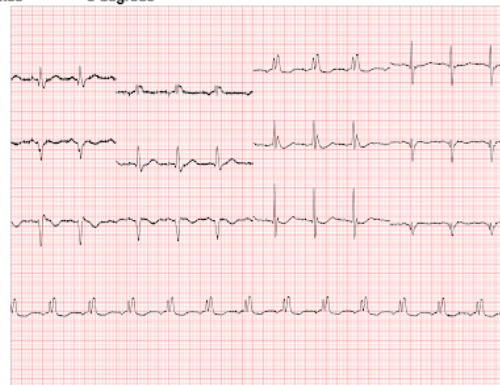
Historically, a calibration DC pulse of 1 mV amplitude and 0.2 s width is also shown on most paper ECGs [29]. Most paper ECG records are of a reddish-orange colour, however this is not standardized. The typical paper ECG record is plotted on A4 or US Letter sized papers. The standard surface ECG is recorded by placing 12 electrodes on 12 different locations on the body, in addition to reference leads. Leads I, II, III, aVR, aVF and aVL denote the leads placed on the limb whereas the leads V1-V6 denote the precordial leads. Reduced ECG lead sets, measure fewer number of leads and reconstruct the other leads by calculation [30], or more recently by machine and deep learning [31], [32].

Most standard paper ECG records contain all the 12 leads plotted along four rows. The V1 (or V2) lead is plotted separately in the 4th row as a 12 s continuous strip, for rhythm analysis. Although majority of paper ECG records follow these practices, there do exist paper ECG records that do not adhere to this. Consequently, a synthetic paper ECG generation pipeline



(a) With lead names

Date:	12-Lead 1	HR 37 bpm	Abnormal ECG unconfirmed
Name:	82 Feb 99	17:81:49	Junction bradycardia found
Identifier:	PR 0.000s	QRS 0.104s	Incomplete right bundle
Age: 82	QT/QTc	0.562s/0.441s	Inferior infarction age undetermined
P-QRS-T Axes	8 degrees		
aVR			



(b) With text artifacts

Fig. 3: Distortion-less synthetic ECG images with lead names (left) and printed text (right)

must take into account the variability that exists across real paper ECG records. Our developed ECGGen toolbox, allows the user to tweak these variabilities and generate a diverse dataset.

### C. Printed text artifacts

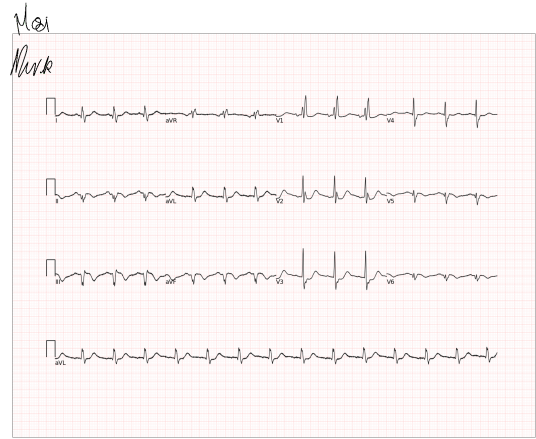
Typically, text artifacts on paper ECG records could contain lead names, patient information/ID, ECG calibration, date, physician's name, diagnostic codes/keywords, ECG-based measurements, and some medical terminologies. Several state and federal regulations, such as the Privacy Rule of the Health Insurance Portability and Accountability Act (HIPAA), mandate the protection of patient privacy [33]. Consequently, in most paper ECG records available, protected health information (PHI) is redacted to preserve privacy. The synthetic paper ECG generation pipeline must accommodate these variable printed text artifacts.

In ECGGen, the lead names (I, II, III, V1, V2, V3, V4, V5, V6, avL, avF, avR) are printed alongside their respective ECG segments on the synthetically generated ECG image (cf. Fig. 3a). The user of the toolbox has the option of choosing whether there must be an overlap between ECG segments and printed text artifacts. Although overlapped characters do pose a problem in digitizing paper ECG records [34], they are added to represent realistic paper ECGs. Further, to add other printed information such as date, ECG calibration, patient record numbers, etc. we have designed several template ECG record files that can be customized by the user. These text are superimposed on the synthetically generated ECG image obtained from the previous step (cf. Fig. 3b).

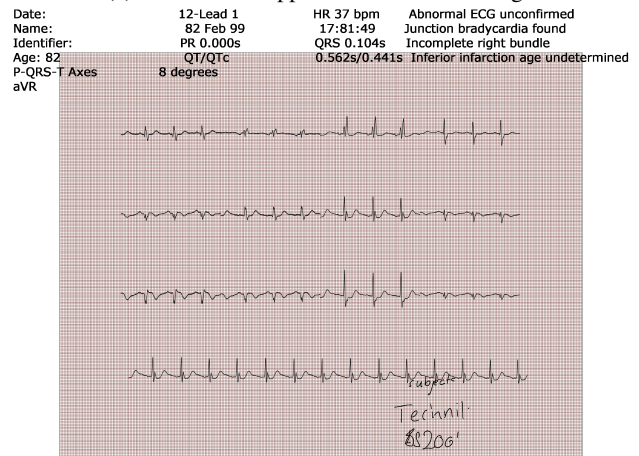
### D. Handwritten text artifacts

Scanned ECGs may contain annotations or hand-written diagnoses from the healthcare provider. Our synthetic ECG image generation pipeline attempts to simulate such handwritten text artifacts to generate more realistic ECG images.

Most handwritten text on paper ECG records comprise of medical terms related to cardiology. We collected a set of medical text related to ECG and CVDs. We next applied Natural Language Processing (NLP) models on these text to compile a list of biomedical phrases and keywords from these texts. The resulting set was converted to handwritten style images using pretrained models and the resulting images were overlaid on the ECG images from the previous step of our pipeline. The Python-based `en_core_sci_md` model from `sciSpacy` [35], was used for the NLP step, which provides a fast and efficient pipeline to perform tokenization, parts of speech tagging, dependency parsing and names entity recognition. Next, the `SpaCy` model [36] was retrained on our collected medical texts to retain words in the ECG-CVD context. The dependency parser and the parts of speech tagger in the released models were retrained on the treebank of McClosky and Charniak [37], which is based on the GENIA 1.0 corpus [38]. Major named entity recognition models have been trained on the MedMentions dataset [39]. Our developed synthetic ECG image generation toolbox parses words from an input text file or from online links using the BeautifulSoup library [40], performs parts of speech tagging on the parsed words and then uses named entity recognition from the aforementioned models to identify ECG-related keywords, which are randomly chosen and add as handwritten text.



(a) Artifacts on upper left corners of image



(b) Artifacts on lower right corner of image with printed text artifacts

Fig. 4: Handwritten text artifacts on synthetic paper ECG

The extracted words need to be converted into handwritten-style text to overlay on the synthetic ECG image. A pretrained Recurrent Neural Network (RNN) transducer-based model paired with soft window is used to generate handwritten text from the extracted words [41]. One of the major challenges in converting the words to handwritten text is that the input and output sequences are of very different lengths dependent on the handwriting style, pen size, etc. The RNN transducer based model is capable of predicting output sequences which are of different length and unknown alignment from the input sequence [42]. The soft window is used to determine the length of the output handwritten sequence by convolving with the input text string. This results in outputs of different lengths for different handwriting styles. Our current handwritten text pipeline allows the user to choose from seven different handwriting styles to overlay onto the ECG image. The coordinates to overlay the text can be chosen by the user of the toolbox, and if not specified are selected randomly. Examples of the resulting images are shown in Fig. 4.

---

**Algorithm 1** Crease Artifacts Generation
 

---

**Require:** Number of creases  $n$ , angle of inclination  $\theta$ , ECG image width  $w$ , ECG image height  $h$

**Ensure:** Crease coordinates:  $start\_points, end\_points$

- 1: Initialize empty arrays  $start\_points, end\_points$
- 2: Calculate the gap between creases:  $gap \leftarrow (w+h)/(n+1)$
- 3: Set  $x_c \leftarrow 0, y_c \leftarrow 0, x_e \leftarrow 0, y_e \leftarrow 0$
- 4: **for**  $i$  in 1 to  $n$  **do**
- 5:   **if**  $(x_c + gap) < w$  **then**
- 6:      $x_c \leftarrow x_c + gap$
- 7:   **else**
- 8:      $y_c \leftarrow x_c + gap - w$
- 9:      $x_c \leftarrow w$
- 10:   **end if**
- 11:   Append  $[x_c, y_c]$  to  $start\_points$
- 12: **end for**
- 13: **for**  $i$  in 1 to  $n$  **do**
- 14:    $x \leftarrow x_c$  from  $start\_points[i]$
- 15:    $y \leftarrow y_c$  from  $start\_points[i]$
- 16:    $m \leftarrow \tan(\pi - \theta)$
- 17:    $c \leftarrow y - m \cdot x$
- 18:    $y_e \leftarrow m \cdot x_e + c$
- 19:   Append  $[x_e, y_e]$  to  $end\_points$
- 20: **end for**
- 21: **return**  $start\_points, end\_points$

---

### E. Paper wrinkles and creases

Wrinkles and creases are very common distortions observed on scanned paper-based ECG images. Wrinkle distortions are caused by the uneven surface of the wrinkled document. When the scanner light passes over the uneven surface, the resulting image can be distorted by shadows or reflections from the wrinkles. This can cause areas of the image to appear darker or lighter than the actual paper, or it can cause the image to appear blurry or distorted. Creases, on the other hand, are caused by the physical crease in the scanned paper. When the scanner light passes over the crease, it can create a shadow that appears as a dark line in the resulting image. This can make the text or image on the creased area difficult to read or interpret.

Wrinkles and creases can be modeled using image processing techniques. Creases can be modeled by Gaussian-distributed blurred lines, linearly spaced to give an impression of creases caused by paper folds. Mathematically, to introduce crease artifacts in an image, the coordinates of the creases can be determined using line equations and translations. To generate the line equations representing creases and to determine their starting and ending points based on the number of creases, their angle of inclination, and the width and height of the image, the steps in Algorithm 1 were taken. This algorithm provides us with the coordinates of the creases using line equations and translation, ensuring that the creases are within the image bounds and contributing to the generation of realistic crease artifacts in the synthetic paper-like ECG images.

To simulate the effect of blurring on crease lines, we apply Gaussian blurring to the generated crease lines, which is

commonly used as an image augmentation technique to simulate smoothing or blurring effects in images. It has also been used to simulate the effect of unfocused camera on the object of interest, which is known to impact the performance of deep neural networks [43]. The blurring process is mathematically expressed as a convolution of the crease lines with a Gaussian kernel:

$$G(x, y) = \frac{1}{2\pi\sigma^2} e^{-\frac{x^2+y^2}{2\sigma^2}} \quad (1)$$

where  $x$  and  $y$  represent the coordinates in the 2D space, and  $\sigma$  represents the standard deviation of the Gaussian distribution in pixels. The application of Gaussian blurring to the created crease lines aids in generating more realistic images by simulating a shadow effect in the crease, which is commonly observed in scanned paper ECG images.

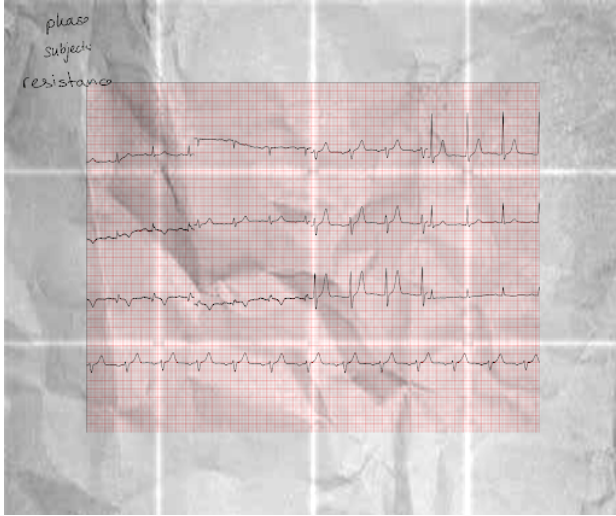
Wrinkles can be thought of as textures and can thus be synthesized by state-of-the-art texture synthesis techniques such as *image quilting* [44]. Image quilting starts with a plain wrinkle image as a seed, followed by randomly selecting a patch from this image. This patch serves as the basis for synthesizing the entire wrinkle texture. Multiple such patches are generated and seamlessly blended using the minimum boundary error cut method [45]. In this method, the goal is to find the optimal boundary between two patches by minimizing the error in the overlap region. The minimum cost path through the region of overlap is found using dynamic programming according to the algorithm proposed in [46]. Instead of using a straight line between the two patches, this method calculates the minimum cost path that represents the boundary of the new block. By doing so, the placement of texture patches appears smoother and more realistic, effectively reducing noticeable sharp edges between the patches.

Let  $B_1$  and  $B_2$  be two blocks that overlap along their vertical edges, and let  $B_{ov1}$  and  $B_{ov2}$  be the regions of overlap between them. The error surface  $e$  is defined as the squared difference between  $B_{ov1}$  and  $B_{ov2}$ :  $e = (B_{ov1} - B_{ov2})^2$ . The error surface  $e$  is traversed for each row ( $i = 2, \dots, N$ ) in the overlapping region and the minimum error path  $E$  is computed using dynamic programming as follows:

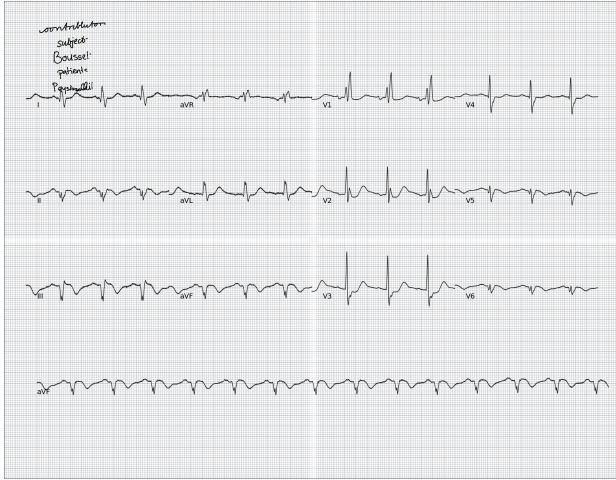
$$E_{i,j} = e_{i,j} + \min(E_{i-1,j-1}, E_{i-1,j}, E_{i-1,j+1}) \quad (2)$$

where  $E_{i,j}$  represents the cumulative minimum error at position  $(i, j)$  in the error matrix  $E$ . The minimum error path is determined by taking the minimum of the three adjacent pixels in the previous row ( $i - 1$ ) and adding it to the corresponding pixel in the current row ( $i$ ). The last row of  $E$  contains the minimal value and hence, the end of the minimal vertical path through the error surface. Backtracking can be used from the last row to determine the path of the best-fit boundary between  $B_1$  and  $B_2$  [44]. Thus a seamless and visually coherent texture is synthesized.

This image quilting technique, combined with the minimum boundary error cut method, helps generate a realistic paper-based texture with wrinkles and creases. Thus the resultant image exhibits natural and realistic blending, contributing to the overall authenticity of the synthetic ECG images. Together,



(a) Wrinkles and creases



(b) Crease artifacts

Fig. 5: Wrinkle and crease artifacts on synthetic ECG images

wrinkles and creases are added as cumulative transforms on the ECG image to add realistic distortions, as shown in Fig. 5.

#### F. Perspective artifacts

We apply perspective transformations on the synthetic paper ECG image to incorporate different camera viewpoints that could have been used while scanning or taking pictures of paper ECG records. Traditionally perspective transformations have been widely used in image augmentation for several vision-based applications. [47] refer to the use of perspective transformations for data augmentation to produce new images captured from different camera viewpoints, specifically for object detection applications. Perspective transforms are simulated by applying geometric transformations to distortionless ECG images. Affine, projective, or homography transformations are utilized to introduce variations in scaling, rotation, and skewing, mimicking the perspective distortions encountered in real paper ECGs. Affine transformations preserve parallelism of lines and can be used to simulate translations, scaling, rotations and shear transformations. Thus, they simulate parallel movements of a

camera when scanning a paper ECG. Given an ECG image, the affine transformation can be represented by the matrix transform:

$$\begin{pmatrix} x' \\ y' \\ 1 \end{pmatrix} = \begin{pmatrix} a & b & c \\ d & e & f \\ 0 & 0 & 1 \end{pmatrix} \begin{pmatrix} x \\ y \\ 1 \end{pmatrix} \quad (3)$$

where  $(x, y)$  are the coordinates of a pixel in the original image  $I$ , and  $(x', y')$  are the transformed coordinates after the affine transformation.

Projective transformations, on the other hand, can be used to simulate skew transformations as well. The affine transformation is a special case of a projective transformation. Projective transformations do not preserve parallelism and can be used to simulate how perceived images change when the view point of the observer changes. Thus, projective transformations are also incorporated into the synthetic paper ECG generation pipeline to account for such perceived observational changes for mobile- or camera-based ECG images. For a projective transformation, also known as a perspective transformation, the matrix equation is given by:

$$\begin{pmatrix} x' \\ y' \\ w' \end{pmatrix} = \begin{pmatrix} a & b & c \\ d & e & f \\ g & h & i \end{pmatrix} \begin{pmatrix} x \\ y \\ 1 \end{pmatrix} \quad (4)$$

where  $(x, y)$  are the coordinates of a pixel in the original ECG image  $I$ ,  $(x', y')$  are the transformed coordinates after the projective transformation, and  $w'$  is a scaling factor that ensures homogeneous coordinate representation. The elements  $a, b, c, d, e, f, g, h,$  and  $i$  in the transformation matrix control the scaling, rotation, shear, skew and perspective effects applied to the image. These transformations add depth and simulate different viewing angles and positions, further enhancing the resemblance to real ECG images.

The above mentioned transforms are performed using the `imgaug` library, available on Python [48]. `imgaug` is a library for image augmentation in machine learning experiments. It supports a wide range of augmentation techniques, allows to easily combine these and to execute them in random order. Thus it can be suitably used for generating synthetic ECG images as a highly variable dataset.

#### G. Imaging artifacts and noise

The final distortions added to the synthetic paper ECG images include imaging noise modeled by Gaussian noise, Poisson noise, salt and pepper noise, and color temperatures, which are essential tools for generating realistic synthetic images and improving the robustness of machine and deep learning models trained on these images. Typically, Gaussian noise arises in digital images during image acquisition, which in this case refers to scanning or taking pictures of paper ECG images or ECG images from a monitor. Gaussian noise, which models sensor noise, is added to each pixel independently:

$$I_{\text{noisy}}(x, y) = I(x, y) + N_{\text{gaussian}}(0, \eta) \quad (5)$$

where  $I_{\text{noisy}}(x, y)$  represents the noisy pixel value,  $I(x, y)$  is the original pixel value of the ECG images, and  $N_{\text{gaussian}}(0, \eta)$

is a random value drawn from a Gaussian distribution with mean 0 and standard deviation  $\eta$ .

Poisson-distributed noise, is commonly used to model noises due to electromagnetic interference during image acquisition, can be added to each pixel:

$$I_{\text{noisy}}(x, y) = \min\{255, \max[0, I(x, y) + N_{\text{poisson}}(\lambda)]\} \quad (6)$$

where  $N_{\text{poisson}}(\lambda)$  is a random value drawn from a Poisson distribution with parameter  $\lambda$ , and clip ensures the pixel value stays within the range  $[0, 255]$  (for 8-bit per color image representations).

Salt and pepper noise models camera sensor malfunction, which may happen when scanning the ECG images. Salt and pepper noise randomly sets pixels to either the minimum or maximum intensity:

$$I_{\text{noisy}}(x, y) = \begin{cases} 0, & \text{with probability } p/2 \\ 255, & \text{with probability } p/2 \\ I(x, y), & \text{with probability } 1 - p \end{cases} \quad (7)$$

where the probability  $p$  determines the density of salt and pepper noise.

Finally, color temperatures can be simulated by adjusting the color channels of the image. A color temperature value is selected and the color channels are transformed using appropriate algorithms such as color temperature scaling or white balance adjustment to mimic the desired color temperature effect. The RGB values of the image are also changed in accordance to a temperature value ranging between 1000 to 40000 Kelvin. The lower values correspond to bluish tinges and the higher values correspond to orangish tinges.

In the developed toolbox, all these artifacts are added in user-adjustable proportions to the synthetic ECG image using the `imgaug` library in Python.

#### IV. CASE STUDY: A DEEP LEARNING MODEL FOR ECG IMAGE DIGITIZATION

As a use case, we used our synthetic ECG image generation toolbox to generate a diverse ECG image dataset to train a deep learning-based ECG image digitization architecture that has demonstrated good performance on real ECG images. The deep model consists of a denoising CNN (DnCNN), followed by post-processing algorithms to recover the ECG time-series data. This model was trained on a dataset of synthetic paper ECG images generated from the PTB diagnostic ECG database time-series [25], consisting of 549 records. The trained model was applied to assess the fidelity of a synthetic paper ECG dataset generated from the PTB-XL dataset [22], consisting of 1000 images.

The histogram of the signal-to-noise ratio (SNR) for recovering the ECG time-series from the synthetic dataset is depicted in Fig. 6, with an average of 27.03 dB and a standard deviation of 2.82 dB. The mean square error (MSE) was computed as an additional metric for comparison, yielding a value of approximately 3.1  $\mu\text{V}$  for PTB-XL ECG dataset, as listed in Table I.

The results demonstrate the effectiveness of the synthetic dataset in generating ECG images for training machine and

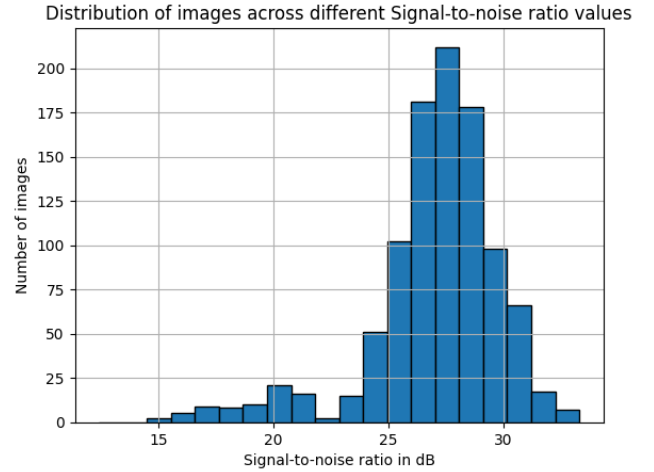


Fig. 6: Histogram of SNR values

TABLE I: Evaluation Results using Deep Learning-based Digitization Algorithm

Metric	Value
Average Signal to Noise Ratio (SNR)	27.03 dB
Standard Deviation of SNR	2.82 dB
Mean Square Error (MSE)	3.1 $\mu\text{V}$
Peak SNR	33.29 dB

deep learning models. The average SNR of 27.03 dB (and a MSE of 3.1  $\mu\text{V}$ ) indicates a high level of similarity between the synthetic paper ECG images and the ground truth time-series data, implying that the generated images closely resemble real paper ECGs. The low standard deviation of 2.82 dB also suggests consistent performance across the dataset, further reinforcing the reliability and stability of the synthetic images. The low MSE of the algorithm in recovering ECG time-series indicates that the algorithm effectively captures the details and characteristics of the ECG waveforms, further validating the fidelity of the synthetic dataset.

Overall, these results affirm the quality and authenticity of the synthetic paper ECG dataset and the effectiveness of the employed digitization algorithm. The findings underscore the significance of utilizing synthetic data for the development and evaluation of digitization algorithms, offering a valuable resource for researchers to explore and improve techniques in ECG analysis and medical diagnostics.

##### A. Computational performance

The dataset generation process was executed in parallel using the HPC cluster of Emory University's Department of Biomedical Informatics (BMI). The cluster is equipped with an NVIDIA DGX1 node to perform computationally intensive operations. The NVIDIA DGX1 node has 80 Intel Xeon E5-2640 v4 CPU cores, a total of 512 GB RAM, and 8 NVIDIA Tesla V100 GPUs, enabling high-performance parallel operations. The dataset generation was distributed across 14 threads on Linux virtual machines. On average, the generation of each synthetic ECG image of size 2200 $\times$ 1700 pixels and 200 dpi resolution took approximately 0.42 s. To provide further

insight into the individual components of the dataset generation pipeline, the required time for each step of the pipeline was also recorded, as detailed in Table II. Accordingly, generating distortionless ECG images (the initial step of the pipeline), took an average of 0.035 s. Subsequently, the addition of handwritten text artifacts required approximately 0.2 s, while wrinkles and creases took around 0.1 s. The application of perspective transforms and augmentation techniques was achieved in approximately 0.065 s per image.

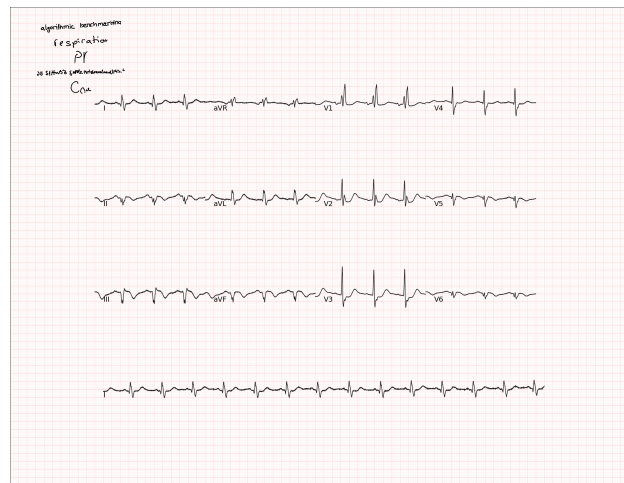
To assess the impact of system specifications, the dataset generation was also conducted on a Windows desktop machine with an Intel 11th Gen Core i7-1165G7 processor, 16 GB of RAM and 10 CPU cores. On this machine, each image (same size and resolution as above) was generated in 27 s. Specifically, distortionless ECG image generation took 2 s, followed by handwritten text artifact addition which required 17 s. The incorporation of wrinkles and creases took approximately 5 s, while perspective transforms and augmentation techniques consumed an average of 4 s.

## V. DISCUSSION

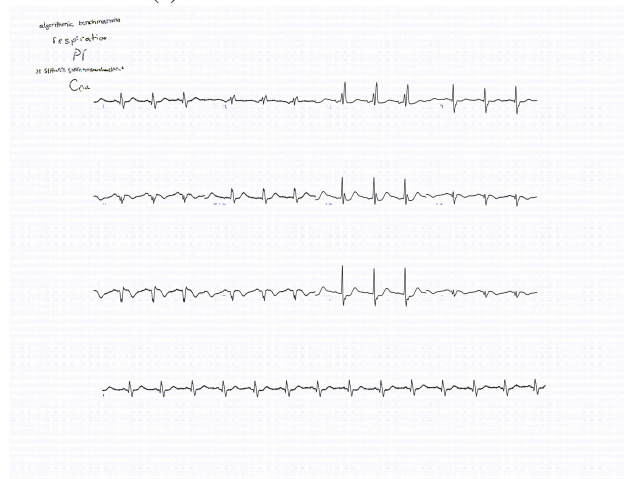
The ECG image digitization results demonstrate the successful synthesis of realistic ECG images that closely resemble the characteristics of real scanned ECG images. The performance evaluation of our pipeline highlights its ability to accurately represent ECG images in a computationally efficient manner. In the sequel, we discuss further steps that could refine the proposed pipeline and optimize its performance for a wider range of machine-learning-based ECG analysis.

According to Table II, the generation of handwritten-like text artifacts is the most time-consuming step of the synthetic ECG image generation pipeline. This is attributed to its RNN transducer-based model, which has 3.4 million parameters [42]. There exist several techniques to shrink the size of a model while achieving acceptable trade-offs on model performance. Future work can entail improving prediction latency using techniques such as freezing, pruning and quantization. Accelerating deep learning inference via freezing has been shown to save potentially 50% of the computation time by halving the number of effective layers [49]. In [50], Molchanov et al. proposed a formulation for pruning convolutional kernels, which resulted in monotonically decreasing inference times. These techniques can be used to prune the handwritten-like image generation step. Quantization of weights can also result in a typical speedup of 2–3 times with tradeoffs in precision for both memory access and computations [51].

Text artifacts in scanned paper ECG images hinder the image digitization performance. A visual inspection of the low performing cases of the ECG digitization pipeline, corresponding to the low-SNR cases on the left tale of the histogram in Fig. 6, revealed that these cases had multiple significant text artifacts, which were not easily discriminated from the ECG traces. This effect is however partially mitigated for the printed text (such as lead names), which are detected by the optical character recognition step. The lowest observed SNR value is 15.12 dB as the corresponding image contained both handwritten and printed text artifacts in huge font sizes, along with wrinkles



(a) With handwritten text artifacts



(b) Post grid removal

Fig. 7: Impact of handwritten text artifacts on digitization of synthetic paper ECG image (recovery SNR=23.67 dB)

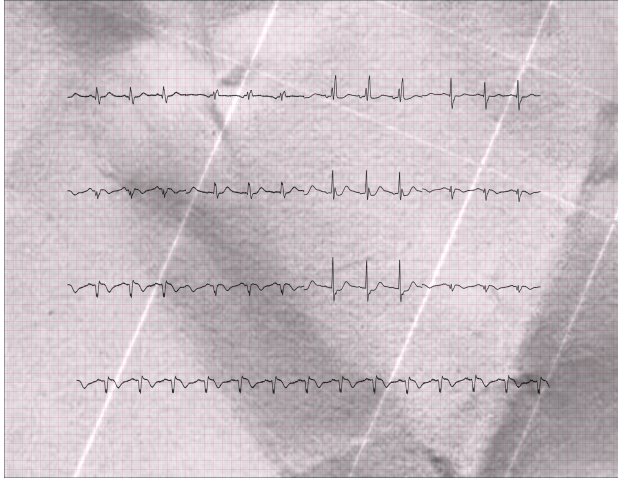
and creases. Typical examples of these corner cases are shown in Fig. 7.

The second step involved addition of wrinkle and crease artifacts. Generating realistic wrinkle-like textures introduces latency to the synthetic image generation process. Image quilting is a computationally intensive process, taking up to an average of 4.71 s per image to generate the textures and another 1.28 s to add wrinkle and crease artifacts (5.99 s in total, see Table II). In [52], Raad et al. propose implementation strategies of the image quilting algorithm using partial parallel processing, allowing a significant speed-up when run with multi-core processors. Incorporating these techniques can significantly reduce the wrinkle generation step run time. Further, Wei et al. in [53] proposed using tree-structured vector quantization for faster texture synthesis that provided nearly 150 times of speedup for certain textures. This technique can further be incorporated in our implementation for faster texture synthesis.

The presence of wrinkles and creases significantly reduces digitization performance. These artifacts, intended to fabricate realistic images resembling real-world paper ECGs, contribute to a reduction in the deep model's performance. The reduced

TABLE II: Average computational time for generating an ECG image of size 2200×1700 pixels and 200dpi on Emory University’s BMI HPC cluster vs a Windows desktop machine (see text for hardware specifications)

Step	BMI cluster time (s)	Desktop machine time (s)
Distortionless ECG Generation	0.035	2.05
Handwritten Text Artifact Addition	0.2	17.11
Wrinkles and Creases Addition	0.1	5.99
Perspective Transforms	0.065	2.03
<b>Total</b>	<b>0.42</b>	<b>27.19</b>



(a) With wrinkles and creases



(b) Post grid removal

Fig. 8: Impact of wrinkles and crease artifacts on digitization of synthetic paper ECG image (recovery SNR=15.43 dB)

SNRs for wrinkle and crease-based distortions range from 15.12 dB to 16.43 dB. This can be attributed to the additional texture and irregularities introduced by these artifacts, which can affect the quality and clarity of the underlying ECG time-series. The observed lower SNR values associated with text artifacts and the inclusion of wrinkles and creases indicate the importance of carefully managing and minimizing the impact of these artifacts during paper ECG scanning and digitization. Sample results of the wrinkle and crease removal step are shown in Fig. 8.

Addition of perspective transforms and imaging noise do

not add significant overhead to the synthetic ECG image generation pipeline. These artifacts are added by traditional image processing techniques that do not require significant computational resources. These artifacts can also be compensated for effectively and do not significantly affect the ECG time-series recovery SNR. This performance is attributed to the denoising Convolutional Neural Network (DnCNN) model, which we employed in the deep-learning based digitization algorithm to remove grid and noise artifacts. This model can handle general image denoising tasks such as blind Gaussian denoising, single image super-resolution with multiple upscaling factors, and JPEG image deblocking with different quality factors [54].

ECG images collected in clinical settings have variable qualities, which depend on the standard practices of acquisition and storage per site. Hence, the images do not always have extreme distortions and are rather consistent in quality and noise/artifact type per clinical setting. Therefore, synthetic datasets used for training ECG digitization models should ideally be generated with similar statistical distributions of these artifacts per site. Future work should incorporate a statistically conscious model-based synthetic ECG generation pipeline for more realistic images. Future research efforts should also focus on developing accurate digitization algorithms and approaches that can effectively mitigate the SNR degradation caused by extreme text artifacts and wrinkles. A practical approach is to pretrain multiple deep models, which are optimized for different scenarios. These models can be deployed in a model, where the user could select between the available models, based on specific needs of each clinical setting.

## VI. CONCLUSION

In this work, we presented a novel approach for generating synthetic paper-like ECG images from time-series data and evaluated the fidelity of the model in a case study for training a deep learning-based ECG image digitization algorithm. The synthetic images have realistic distortions, including handwritten-like text artifacts, wrinkles and creases, and perspective transforms, making them very similar to actual paper ECGs. The evaluation results, which used the signal-to-noise ratio and mean square error (MSE) metrics of the original vs recovered ECG time-series, show that the synthetic ECG image dataset has been indeed effective for building an accurate ECG image digitization pipeline. The high SNR values (low MSE) and visual inspection show a strong resemblance between the generated synthetic images and the ground truth time-series data, assessing the synthetic dataset’s integrity.

The significance of this research lies in its ability to address the challenges associated with limited access to real patient ECG data due to privacy concerns and regulations governing protected health information (PHI). By creating synthetic paper ECG images, researchers can ensure privacy compliance while still enabling the development and testing of ECG analysis algorithms. This proposed method offers a controlled and diverse dataset with realistic distortions, allowing for comprehensive testing and optimization of digitization techniques. Additionally, the synthetic paper ECG dataset serves as a valuable resource for algorithm development and training data augmentation for machine learning models, thereby supporting advancements in medical diagnoses.

Future research in this field could focus on expanding the synthetic paper ECG dataset by incorporating additional forms of distortions and variations, such as electrode misplacements, noise patterns, and heart rate variability. Furthermore, conducting a *Turing test* in collaboration with medical specialists would be beneficial to determine whether the synthetic data generated in this study adequately simulates real medical ECG records. This human evaluation would provide crucial insights into the perceptual fidelity and realism of the synthetic dataset, with measures like the Kappa value being employed to assess agreement between human assessors. Such evaluation would confirm the similarity and reliability of the synthetic data, facilitating its effective integration into clinical settings, with applications in algorithmic ECG annotation and training. Moreover, exploring the utilization of generative adversarial networks (GANs) and other advanced techniques for generating synthetic medical data could enhance the dataset's realism and diversity.

In conclusion, the study presented in this paper lays the foundation for employing synthetic medical data in ECG analysis, opening doors to future advancements in medical diagnostics and contributing to improved patient care.

## REFERENCES

- [1] G. R. Dagenais, D. P. Leong, S. Rangarajan, F. Lanas, P. Lopez-Jaramillo, R. Gupta, R. Diaz, A. Avezum, G. B. F. Oliveira, A. Wielgosz, S. R. Parambath, P. Mony, K. F. Alhabib, A. Temizhan, N. Ismail, J. Chifamba, K. Yeates, R. Khatib, O. Rahman, K. Zatonska, K. Kazmi, L. Wei, J. Zhu, A. Rosengren, K. Vijayakumar, M. Kaur, V. Mohan, A. Yusufali, R. Kelishadi, K. K. Teo, P. Joseph, and S. Yusuf, "Variations in common diseases, hospital admissions, and deaths in middle-aged adults in 21 countries from five continents (PURE): a prospective cohort study," *The Lancet*, vol. 395, no. 10226, pp. 785–794, 2020. [Online]. Available: <https://www.sciencedirect.com/science/article/pii/S0140673619320070>
- [2] R. Rajni and I. Kaur, "Electrocardiogram signal analysis-an overview," *International Journal of Computer Applications*, vol. 84, no. 7, pp. 22–25, 2013.
- [3] K. C. Siontis, P. A. Noseworthy, Z. I. Attia, and P. A. Friedman, "Artificial intelligence-enhanced electrocardiography in cardiovascular disease management," *Nature Reviews Cardiology*, vol. 18, no. 7, pp. 465–478, 2021.
- [4] G. J. Annas, "HIPAA regulations: a new era of medical-record privacy?" *New England Journal of Medicine*, vol. 348, p. 1486, 2003.
- [5] K. El Emam, S. Rodgers, and B. Malin, "Anonymising and sharing individual patient data," *bmj*, vol. 350, 2015.
- [6] K. El Emam, E. Jonker, L. Arbuckle, and B. Malin, "A systematic review of re-identification attacks on health data," *PLoS one*, vol. 6, no. 12, p. e28071, 2011.
- [7] S. Seyedi, L. Xiong, S. Nemati, and G. D. Clifford, "An analysis of protected health information leakage in deep-learning based de-identification algorithms," *ArXiv*, vol. abs/2101.12099, 2021.
- [8] Y. Li, Q. Qu, M. Wang, L. Yu, J. Wang, L. Shen, and K. He, "Deep learning for digitizing highly noisy paper-based ECG records," *Computers in biology and medicine*, vol. 127, p. 104077, 2020.
- [9] J. Weldon, T. Ward, and E. Brophy, "Generation of synthetic electronic health records using a federated GAN," *arXiv preprint arXiv:2109.02543*, 2021.
- [10] E. Choi, S. Biswal, B. Malin, J. Duke, W. F. Stewart, and J. Sun, "Generating multi-label discrete patient records using generative adversarial networks," in *Machine learning for healthcare conference*. PMLR, 2017, pp. 286–305.
- [11] J. Yoon, M. Mizrahi, N. Ghalaty, T. Jarvinen, A. Ravi, P. Brune, F. Kong, D. Anderson, G. Lee, A. Meir, F. Bandukwala, E. Kanal, S. Arik, and T. Pfister, "EHR-safe: Generating high-fidelity and privacy-preserving synthetic electronic health records," Dec. 2022.
- [12] P. E. McSharry, G. D. Clifford, L. Tarassenko, and L. A. Smith, "A dynamical model for generating synthetic electrocardiogram signals," *IEEE transactions on biomedical engineering*, vol. 50, no. 3, pp. 289–294, 2003.
- [13] R. Sameni, G. D. Clifford, C. Jutten, and M. B. Shamsollahi, "Multi-channel ECG and noise modeling: Application to maternal and fetal ECG signals," *EURASIP Journal on Advances in Signal Processing*, vol. 2007, pp. 1–14, 2007.
- [14] G. D. Clifford, S. Nemati, and R. Sameni, "An artificial vector model for generating abnormal electrocardiographic rhythms," *Physiological measurement*, vol. 31, no. 5, p. 595, 2010.
- [15] E. K. Roonizi and R. Sameni, "Morphological modeling of cardiac signals based on signal decomposition," *Computers in Biology and Medicine*, vol. 43, no. 10, pp. 1453–1461, Oct. 2013.
- [16] A. Sološenko, A. Petrėnas, B. Paliakaitė, V. Marozas, and L. Sörnmo, "Model for Simulating ECG and PPG Signals with Arrhythmia Episodes," *Python, Matlab*, 2021.
- [17] F. Zhu, F. Ye, Y. Fu, Q. Liu, and B. Shen, "Electrocardiogram generation with a bidirectional LSTM-CNN generative adversarial network," *Scientific reports*, vol. 9, no. 1, pp. 1–11, 2019.
- [18] A. M. Delaney, E. Brophy, and T. E. Ward, "Synthesis of realistic ECG using generative adversarial networks," *arXiv preprint arXiv:1909.09150*, 2019.
- [19] Y.-H. Zhang and S. Babaeizadeh, "Synthesis of standard 12-lead electrocardiograms using two-dimensional generative adversarial networks," *Journal of Electrocardiology*, vol. 69, pp. 6–14, 2021.
- [20] N. Wulan, W. Wang, P. Sun, K. Wang, Y. Xia, and H. Zhang, "Generating electrocardiogram signals by deep learning," *Neurocomputing*, vol. 404, pp. 122–136, 2020.
- [21] V. Thambawita, J. L. Isaksen, S. A. Hicks, J. Ghouse, G. Ahlberg, A. Linneberg, N. Grarup, C. Ellervik, M. S. Olesen, T. Hansen *et al.*, "Deepfake electrocardiograms using generative adversarial networks are the beginning of the end for privacy issues in medicine," *Scientific reports*, vol. 11, no. 1, p. 21896, 2021.
- [22] P. Wagner, N. Strodthoff, R.-D. Boussejot, D. Kreiseler, F. I. Lunze, W. Samek, and T. Schaeffter, "PTB-XL, a large publicly available electrocardiography dataset," *Scientific data*, vol. 7, no. 1, pp. 1–15, 2020.
- [23] F. Liu, C. Liu, L. Zhao, X. Zhang, X. Wu, X. Xu, Y. Liu, C. Ma, S. Wei, Z. He *et al.*, "An open access database for evaluating the algorithms of electrocardiogram rhythm and morphology abnormality detection," *Journal of Medical Imaging and Health Informatics*, vol. 8, no. 7, pp. 1368–1373, 2018.
- [24] V. Tihonenko, A. Khaustov, S. Ivanov, A. Rivin, and E. Yakushenko, "St Petersburg INCART 12-lead arrhythmia database," *PhysioBank PhysioToolkit and PhysioNet*, 2008.
- [25] R. Boussejot, D. Kreiseler, and A. Schnabel, "Nutzung der EKG-signaldatenbank CARDIODAT der PTB über das internet," *Biomedizinische Technik/Biomedical Engineering*, pp. 317–318, Jul. 1995. [Online]. Available: <https://doi.org/10.1515/bmte.1995.40.s1.317>
- [26] M. A. Reyna, N. Sadr, E. A. P. Alday, A. Gu, A. J. Shah, C. Robichaux, A. B. Rad, A. Elola, S. Seyedi, S. Ansari, H. Ghanbari, Q. Li, A. Sharma, and G. D. Clifford, "Will two do? varying dimensions in electrocardiography: The PhysioNet/computing in cardiology challenge 2021," in *2021 Computing in Cardiology (CinC)*. IEEE, Sep. 2021.
- [27] G. D. Clifford, F. Azuaje, and P. McSharry, "ECG statistics, noise, artifacts, and missing data," *Advanced methods and tools for ECG data analysis*, vol. 6, no. 1, p. 18, 2006.
- [28] G. Moody, W. Muldrow, and R. Mark, "A noise stress test for arrhythmia detectors," *Proceedings of Annual International Conference on Computers in Cardiology*, pp. 381–384, 1984.
- [29] A. Luthra, *ECG made easy*. Jaypee Brothers Medical Publishers, 2019.

- [30] J. A. Malmivuo and R. Plonsey, *Bioelectromagnetism, Principles and Applications of Bioelectric and Biomagnetic Fields*. Oxford University Press, 1995. [Online]. Available: <http://butler.cc.tut.fi/~malmivuo/bem/bembook>
- [31] S. Whyte, K. Farhat, K. Sample, R. Barber, A. Vera, A. Shaw, N. Wells-Serrano, J. Xue, D. Albert, and S. Stavrakis, "Clinical validation of a mobile, artificial intelligence-guided, 12-lead ECG device," *Heart Rhythm*, vol. 20, no. 5, p. S135, May 2023.
- [32] T. Dwivedi, J. Xue, D. Treiman, A. Dubey, and D. Albert, "Machine learning models of 6-lead ECGs for the interpretation of left ventricular hypertrophy (LVH)," *Journal of Electrocardiology*, vol. 77, pp. 62–67, Mar. 2023.
- [33] H. Office for Civil Rights, "Standards for privacy of individually identifiable health information. Final rule," *Federal register*, vol. 67, no. 157, pp. 53 181–53 273, 2002.
- [34] S. Ganesh, P. T. Bhatti, M. Alkhalaf, S. Gupta, A. J. Shah, and S. Tridandapani, "Combining Optical Character Recognition With Paper ECG Digitization," *IEEE Journal of Translational Engineering in Health and Medicine*, vol. 9, pp. 1–9, 2021.
- [35] M. Neumann, D. King, I. Beltagy, and W. Ammar, "ScispaCy: fast and robust models for biomedical natural language processing," *arXiv preprint arXiv:1902.07669*, 2019.
- [36] M. Honnibal and I. Montani, "spaCy 2: Natural language understanding with Bloom embeddings, convolutional neural networks and incremental parsing," *To appear*, vol. 7, no. 1, pp. 411–420, 2017.
- [37] D. McClosky and E. Charniak, "Self-training for biomedical parsing," in *Proceedings of ACL-08: HLT, Short Papers*, 2008, pp. 101–104.
- [38] J.-D. Kim, T. Ohta, Y. Tateisi, and J. Tsujii, "GENIA corpus—a semantically annotated corpus for bio-textmining," *Bioinformatics*, vol. 19, no. suppl\_1, pp. i180–i182, 2003.
- [39] S. Mohan and D. Li, "MedMentions: A Large Biomedical Corpus Annotated with UMLS Concepts," *arXiv preprint arXiv:1902.09476*, 2019.
- [40] L. Richardson, "Beautiful Soup Documentation," Apr. 2023, version 4.12.2. [Online]. Available: <https://www.crummy.com/software/BeautifulSoup/>
- [41] A. Graves, "Generating sequences with recurrent neural networks," *arXiv preprint arXiv:1308.0850*, 2013.
- [42] —, "Sequence transduction with recurrent neural networks," *arXiv preprint arXiv:1211.3711*, 2012.
- [43] S. Dodge and L. Karam, "Understanding how image quality affects deep neural networks," in *2016 eighth international conference on quality of multimedia experience (QoMEX)*. IEEE, 2016, pp. 1–6.
- [44] A. A. Efros and W. T. Freeman, "Image quilting for texture synthesis and transfer," in *Proceedings of the 28th annual conference on Computer graphics and interactive techniques*, 2001, pp. 341–346.
- [45] L. Liang, C. Liu, Y.-Q. Xu, B. Guo, and H.-Y. Shum, "Real-time texture synthesis by patch-based sampling," *ACM Transactions on Graphics (ToG)*, vol. 20, no. 3, pp. 127–150, 2001.
- [46] J. Davis, "Mosaics of scenes with moving objects," in *Proceedings. 1998 IEEE Computer Society Conference on Computer Vision and Pattern Recognition (Cat. No. 98CB36231)*. IEEE, 1998, pp. 354–360.
- [47] K. Wang, B. Fang, J. Qian, S. Yang, X. Zhou, and J. Zhou, "Perspective transformation data augmentation for object detection," *IEEE Access*, vol. 8, pp. 4935–4943, 2019.
- [48] A. Jung, "Imgaug documentation," *Readthedocs.io, Jun*, vol. 25, 2019.
- [49] A. Kumar, A. Balasubramanian, S. Venkataraman, and A. Akella, "Accelerating deep learning inference via freezing," in *HotCloud*, 2019.
- [50] P. Molchanov, S. Tyree, T. Karras, T. Aila, and J. Kautz, "Pruning convolutional neural networks for resource efficient inference," *arXiv preprint arXiv:1611.06440*, 2016.
- [51] R. Krishnamoorthi, "Quantizing deep convolutional networks for efficient inference: A whitepaper," *arXiv preprint arXiv:1806.08342*, 2018.
- [52] L. Raad and B. Galerne, "Efros and Freeman image quilting algorithm for texture synthesis," *Image Processing On Line*, vol. 7, pp. 1–22, 2017.
- [53] L.-Y. Wei and M. Levoy, "Fast texture synthesis using tree-structured vector quantization," in *Proceedings of the 27th annual conference on Computer graphics and interactive techniques*, 2000, pp. 479–488.
- [54] K. Zhang, W. Zuo, Y. Chen, D. Meng, and L. Zhang, "Beyond a gaussian denoiser: Residual learning of deep CNN for image denoising," *IEEE transactions on image processing*, vol. 26, no. 7, pp. 3142–3155, 2017.